ISSN 2070-0504, Catalysis in Industry, 2013, Vol. 5, No. 2, pp. 133–142. © Pleiades Publishing, Ltd., 2013.
Original Russian Text © E.A. Alikin, S.Yu. Bochkarev, S.P. Denisov, N.M. Danchenko, V.N. Rychkov, A.S. Volkov, A.S. Karpov, 2013, published in Kataliz v Promyshlennosti.

CATALYSIS AND ENVIRONMENTAL PROTECTION

Thermally Stable Composite System Al_2O_3–$Ce_{0.75}Zr_{0.25}O_2$ for Automotive Three-Way Catalysts

E. A. Alikin[a], S. Yu. Bochkarev[a], S. P. Denisov[a], N. M. Danchenko[a], V. N. Rychkov[b], A. S. Volkov[b], and A. S. Karpov[b]

[a] *Ecoalliance. Ltd, Novouralsk, Sverdlovsk oblast, 624131 Russia*

[b] *Ural Federal University, Yekaterinburg, 620002 Russia*

Received June 20, 2011

Abstract—Present-day three-way catalysts operate in contact with exhaust gases whose temperature is as high as >1000°C, so the problem of developing thermally stable catalytic compositions is still topical. A series of Al_2O_3–$Ce_{0.75}Zr_{0.25}O_2$ composites containing 0, 10, 25, and 50 wt % Al_2O_3 has been synthesized by direct precipitation. The as-prepared composites and those calcined in air at 1000 and 1100°C have been characterized by BET, X-ray diffraction, transmission electron microscopy, and temperature-programmed reduction methods. The composites aged at 1050°C in a 2% O_2 + 10% H_2O + 88% N_2 atmosphere have been used to prepare monolith catalysts, and the oxygen storage capacity (OSC) of the latter has been measured using a gas analysis setup. As the proportion of Al_2O_3 in the composite is raised, the mixing uniformity and degree of dispersion of $Ce_xZr_{1-x}O_{2-\delta}$ particles increase, their chemical composition becomes homogeneous, and the amount of cerium involved in oxidation and reduction increases. The composite containing 50 wt % Al_2O_3 is a mixture of $Ce_xZr_{1-x}O_{2-\delta}$ and Al_2O_3 crystallites, whose size is practically unaffected by calcination. The (Pt/Al_2O_3 + Al_2O_3–$Ce_{0.75}Zr_{0.25}O_2$) based on this composite has the highest OSC and is the most active. For this reason, full-scale testing of this catalyst is recommended.

Keywords: three-way catalyst, thermal stability, composite, OSC, crystallites

DOI: 10.1134/S2070050413020025

INTRODUCTION

The problem of abating hazardous emissions (CO, CH_x, NO_x) from spark-ignition engines is traditionally solved by using a three-way catalyst (TWC). The purpose of a TWC is to simultaneously convert CH_x and NO_x into CO_2, H_2O, and N_2. TWCs contain platinum-group metals (Pt, Pd, Rh) supported on a mixed material consisting of alumina and cerium-containing oxides [1].

Three-way catalysts operate under stoichiometric fuel combustion conditions. As the engine runs, the oxygen concentration in the exhaust gas varies. Use of cerium-containing materials is dictated by the ability of cerium ions to undergo partial reduction and oxidation in response to the variation of oxygen concentration in the gas phase. This property, which is characterized by oxygen storage capacity (OSC), makes the TWC capable of counterbalancing the oxygen concentration variations in the exhaust (which are due to the specific features of engine operation) by maintaining a near-stoichiometric amount of oxygen on the catalyst surface. This allows simultaneous oxidation and reduction reactions to proceed efficiently.

The activity of a catalyst exposed to high-temperature (>1000°C [2]) exhaust declines mainly because of aggregation processes taking place: the specific surface area of Al_2O_3 and CeO_2 decreases, and so does the OSC of CeO_2, and the platinum-group metals undergo sintering. For efficient operation of a catalyst, its specific surface area and OSC should be maintained at 40–100 m^2/g and 0.1–0.25 mmol O/g, respectively.

Cerium dioxide sinters at 700–800°C [3, 4]. The most common way of enhancing the OSC and thermal stability of CeO_2 is by preparing its solid solution with ZrO_2 with a fluorite structure [5]. It was established that $Ce_xZr_{1-x}O_{2-\delta}$ with $x = 0.5$–0.8 ($\delta = 0$–0.25) has the highest dynamic OSC (0.219 mmol O/g) and high thermal stability (specific surface area of 30–40 m^2/g after annealing at $T = 900$°C for 6 h) [6–8]. However, the solid solution is metastable at these Ce/Zr ratios. In particular, cubic $Ce_xZr_{1-x}O_2$ ($x = 0.5$–0.8) turns into a tetragonal phase richer in zirconium at 1000–1100°C [9].

Doping of Al_2O_3 with certain elements slows down its phase transitions and enhances its thermal stability [10]. These dopants include cerium [11, 12] and zirconium [10, 11]. In the case of both components simultaneously introduced into alumina by impregnation, the stabilizing effect is stronger than in the case of doping with cerium alone. Furthermore, alumina favors the formation of $Ce_xZr_{1-x}O_{2-\delta}$, which has a higher OSC than individual zirconium oxide, and allows high

OSC values to be retained after annealing at 1000–1100°C [13, 14]. Simultaneous doping of alumina with zirconium and cerium inhibits the undesired interaction between CeO_2 and Al_2O_3, preventing the formation of cerium aluminate $CeAlO_3$ [15].

Using the coprecipitation method, it is possible to synthesize Al_2O_3–$Ce_xZr_{1-x}O_{2-\delta}$ oxide compositions that are characterized by a higher thermal stability of the phases and have a higher OSC than the mechanical mixture of Al_2O_3 and $Ce_xZr_{1-x}O_{2-\delta}$ powders [16, 17]. Owing to its high melting point and chemical inertness, alumina is a textural promoter. The uniformity of mixing of Al_2O_3 and $Ce_xZr_{1-x}O_{2-\delta}$ depends on the ratio of their concentrations and on the composite preparation conditions. In the limiting case of component mixing on the individual crystallite scale, there will be the strongest mutual promoting effect.

Aimed at obtaining the thermally most stable oxide system, we synthesized a series of Al_2O_3–$Ce_{0.75}Zr_{0.25}O_{2-\delta}$ composites with various Al_2O_3-to-$Ce_{0.75}Zr_{0.25}O_{2-\delta}$ ratios and studied the physicochemical properties and activity of catalysts based on these materials.

EXPERIMENTAL

The individual oxide $Ce_{0.75}Zr_{0.25}O_{2-\delta}$ (CZ) and a series of Al_2O_3–$Ce_{0.75}Zr_{0.25}O_{2-\delta}$ composites with Al_2O_3-to-$Ce_{0.75}Zr_{0.25}O_{2-\delta}$ weight ratios of 1 : 9 (A10-CZ), 1 : 3 (A25-CZ), and 1 : 1 (A50-CZ) were prepared by direct precipitation. Solutions of Ce^{3+}, ZrO^{2+}, and Al^{3+} nitrates were combined in preset proportions. The total concentration of the components was 100 g/L. The oxides were precipitated from the mixed solution by adding aqueous ammonia (C = 25%) dropwise under stirring. The hydroxide mixture together with the mother liquor was held at 100°C for 120 h at atmospheric pressure. Thereafter, the precipitates were filtered and were repulped in isopropanol. The resulting pasty materials were dried at 100°C for 12 h and were calcined at 500°C for 2 h.

The elements in the synthesized materials were quantified by atomic absorption spectrometry on an Optima 4300 DV spectrometer.

Physicochemical properties were determined for as-prepared samples and for samples calcined at 1000°C for 1 h in air.

The specific surface area and pore structure parameters were determined by low-temperature nitrogen adsorption/desorption using an ASAP 2400 analyzer.

X-rays diffraction patterns were recorded on a Rigaku ULTIMA IV diffractometer (CuK_α radiation) using a scintillation counter with a monochromator crystal placed in the diffracted beam ($2\theta = 0.05°$ steps, counting time of 5 s per data point). The crystallite size was calculated by the Williamson–Hall method using the Scherrer formula.

Transmission electron microscopy (TEM) studies were carried out on a JEM-2010 microscope with a lattice resolution of 0.14 nm. The elemental composition of the materials was determined by X-ray microanalysis (EDX) using an EDX energy-dispersive spectrometer fitted with a Si(Li) detector with an energy resolution of 130 eV and a microprobe spot size down to 10 nm. The specimen was mounted on a 10- to 20-nm-thick holey carbon film affixed to a copper grid.

The temperature-programmed reduction (TPR) of materials in hydrogen was performed in a flow reactor. Prior to recording a TPR spectrum, the sample was held in flowing argon for 3–5 min. The spectra were recorded while heating the sample from room temperature to 900°C at a rate of 10 deg/min in a 10 vol % H_2 + 90 vol % Ar mixture flowing at a rate of 40 mL/min. Two spectra were obtained for each sample; between the runs, the sample was exposed to flowing oxygen at 500°C for 30 min. The data obtained in the second run were used in the analysis. From this experiment, we derived the total amount of hydrogen (mmol) taken up by the sample under linear heating in the 40–900°C range.

The dynamic OSC of cerium-containing oxides was measured in a monolith catalyst. For a direct intercomparison of oxides to be possible, the monolith samples were loaded with equal amounts of $Ce_xZr_{1-x}O_{2-\delta}$ at a fixed weight of the catalyst layer. For this purpose, an additional amount of Al_2O_3 was added to CZ, A10-CZ, and A25-CZ so as to adjust the alumina content of all oxide materials to 50 wt %. Next, the materials were aged at 1050°C for 4 h in an oxygen- and water-containing nitrogen atmosphere (2% O_2 + 10% H_2O + 88% N_2). Thereafter, the materials were mixed with the Pt(0.8%)/Al_2O_3 catalyst in a weight ratio of 45 : 55 and suspensions of the resulting mixture were prepared, which were then deposited onto a honeycomb cordierite support (diameter of 25.4 mm, length of 101.6 mm, 63 cells per square centimeter). The weight of the catalyst layer in the honeycomb catalysts was 4.6 g, the weight of $Ce_{0.75}Zr_{0.25}O_2$ was 1 g, and the weight of Pt was 0.02 g.

Oxygen storage capacity was measured using a Horiba CTSJ-2003.12 analytical setup by the response method in CO oxidation [18]. The following mixture was passed through the catalyst sample: O_2, 0 or 1 vol %; CO, 0.65 vol %; CO_2, 9.35 vol %; N_2 balance; GHSV = 20000 h^{-1}. The oxygen concentration was changed from zero to its maximum value (1%) at 100-s intervals. The gas mixture was heated in the reactor from 100 to 500°C at a rate of 5°C/min using an electric heater. The OSC value (mmol) in each run was determined in the zero oxygen concentration period as the amount of atomic oxygen released by the monolith sample per unit weight of CeO_2 (on the basis of the stoichiometry of the CO + O = CO_2 reaction).

Catalytic activity was measured for monolith samples prepared for OSC measurements. It was estimated

Table 1. Characteristics of the CZ, A10-CZ, A25-CZ, and A50-CZ composites

Parameter	Composite			
	CZ	A10-CZ	A25-CZ	A50-CZ
Al_2O_3 of the composite according to atomic absorption spectroscopy data, wt %	–	10	23	46
Specific surface area, m^2/g:				
as-prepared	93	94	103	166
calcined at 1000°C	31	30	52	86
Pore volume, cm^3/g:				
as-prepared	0.304	0.288	0.567	0.702
calcined at 1000°C	0.200	0.175	0.422	0.598
Mean pore diameter, Å:				
as-prepared	112	110	185	130
calcined at 1000°C	213	204	273	213
Unit cell parameter, Å:				
as-prepared (500°C)	5.3855	5.3843	5.3811	5.3607
calcined at 1000°C	5.3751	5.3983	5.3905	5.3735
calcined at 1100°C	5.3707	5.3999	5.4088	5.3738
Crystallite size, nm:				
as-prepared (500°C)	9	7	8	8
calcined at 1000°C	16	15	12	14
calcined at 1100°C	24	21	17	16

in terms of the temperature of 50% CO, CH_x, and NO_x conversion. The following mixture was fed to the monolith catalyst: O_2, 1.15 vol %; CO, 1.60 vol %; NO_x, 1000 ppm; C_3H_6, 250 ppm; C_3H_8, 250 ppm; CO_2, 9.35 vol %; H_2O, 10 vol %; H_2, 0.4 vol %; N_2 balance; GHSV = 30000 h^{-1}.

RESULTS AND DISCUSSION

Textural Characteristics and Morphology

The textural characteristics of the synthesized materials are listed in Table 1. The A10-CZ and CZ samples have practically equal specific surface areas in both as-prepared and calcined states. The samples that are richer in alumina (A25-CZ and A50-CZ) have a larger specific surface area and a larger pore volume. It is likely that 10 wt % Al_2O_3 is insufficient for textural promotion and alumina makes a significant contribution to the specific surface area when its percentage is high. The mean pore diameter is practically invariable over the sample series, except for A25-CZ. For the calcined samples, the mean pore diameter of the material richest in Al_2O_3 (A50-CZ) is equal to that of the Al_2O_3-free material (CZ).

The X-ray diffraction patterns of the as-prepared and calcined samples show reflections from a solid solution with a fluorite structure, which is characteristic of the $Ce_xZr_{1-x}O_{2-\delta}$ compound (Fig. 1). The unit cell parameters of all samples are larger than the reference value for $Ce_{0.75}Zr_{0.25}O_2$ (5.3490 Å according to ICDD 00-028-0271 1). This may be due to the typical presence of Ce^{3+} cations, which have a larger ionic radius than Ce^{4+} (1.14 and 0.97 Å, respectively [19]), and to the deviation of the chemical composition of the synthesized phase from the theoretical formula $Ce_{0.75}Zr_{0.25}O_2$. The latter hypothesis is partially corroborated by the observation of reflections from tetragonal ZrO_2 for calcined CZ, A10-CZ, and A25-CZ. These reflections appear as a shoulder at the strongest reflections from $Ce_xZr_{1-x}O_{2-\delta}$—(111) and (220). The tetragonal phase is not detected in A50-CZ calcined at 1100°C (Fig. 1).

As the alumina content is increased, the reflections from $Ce_xZr_{1-x}O_{2-\delta}$ in the diffraction pattern of the materials weaken; however, alumina is detected only in calcined A50-CZ as its (400) and (440) reflections.

The $Ce_xZr_{1-x}O_{2-\delta}$ crystallite size in all materials increases with an increasing heat-treatment temperature (Table 1). In the samples aged at 1100°C, there is a stabilizing effect of Al_2O_3, which shows itself as the crystallite size decreasing with an increase in the Al_2O_3 content. The smallest crystallite size is observed in A50-CZ.

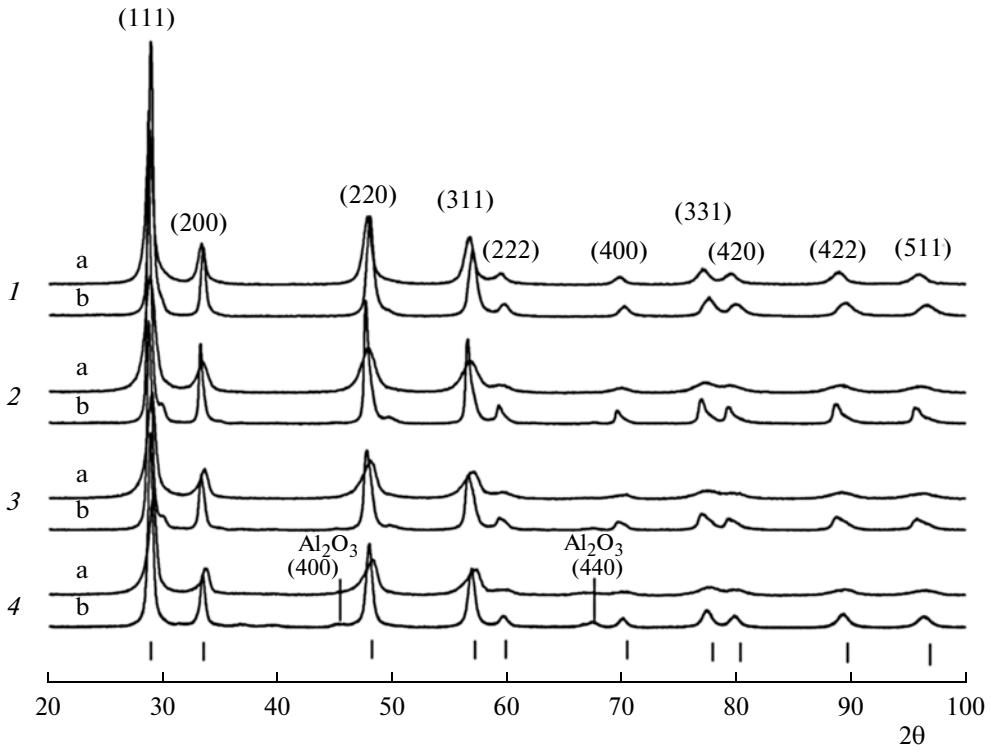

Fig. 1. X-ray diffraction patterns of (a) as-prepared composites and (b) the same composites calcined at 1000°C: (*1*) CZ, (*2*) A10-CZ, (*3*) A25-CZ, and (*4*) A50-CZ. The vertical lines indicate the positions of reflections from $Ce_{0.75}Zr_{0.25}O_2$ (ICDD 00-028-0271).

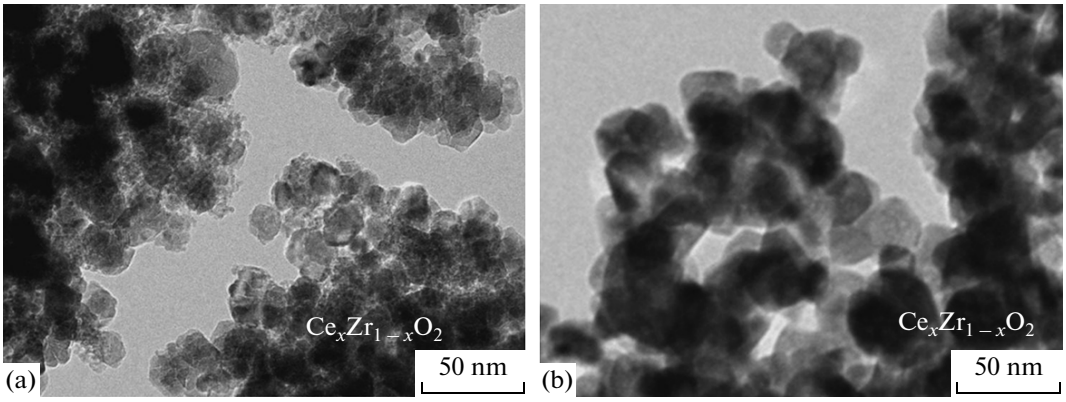

Fig. 2. TEM image of (a) as-prepared CZ and (b) the same material calcined at 1000°C.

The morphology of as-prepared CZ is characterized by the presence of 100-nm and larger aggregates consisting of isometric 20–30 nm particles (Fig. 2). A microprobe analysis of these particles demonstrated that the average Ce : Zr ratio is 82 : 18. In the vicinity of interblock boundaries, there is a finely dispersed oxide fraction with a particle size of ≈2–5 nm, in which the proportion of zirconium is above average, with Ce : Zr = 63 : 37.

The particles of calcined CZ are faceted, with a dominant size of about 20 nm; however, larger crystals (up to 50 nm) are also observed, which result from sintering (Fig. 2). There are no finer particles in aged CZ. An elemental analysis of this material demonstrated that the particles about 20 nm in size have approximately the same composition and are richer in zirconium than the larger ones (~50 nm). The sintering of CZ resulted in a more uniform distribution of Zr in the binary oxide.

In as-prepared A10-CZ (Fig. 3), there are large, elongated, spongy Al_2O_3 aggregates up to 1 μm in length, ~300 nm in width, and 5 nm in thickness. The

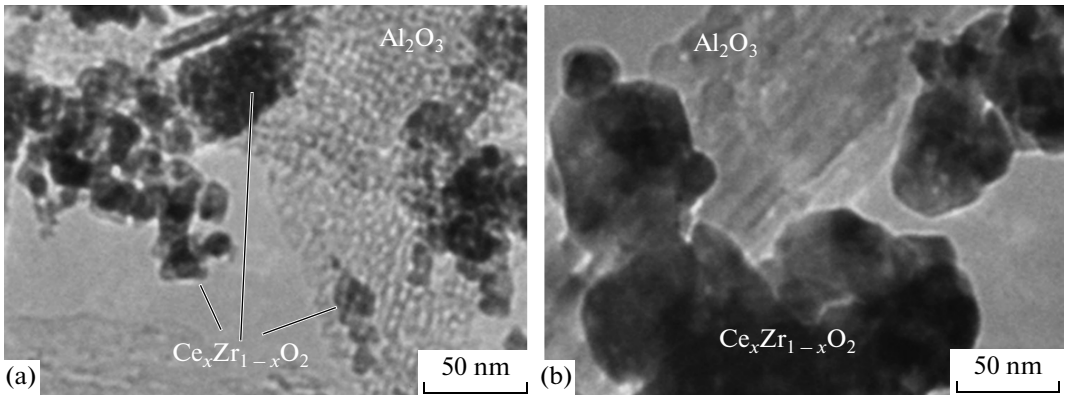

Fig. 3. TEM image of (a) as-prepared A10-CZ and (b) the same material calcined at 1000°C.

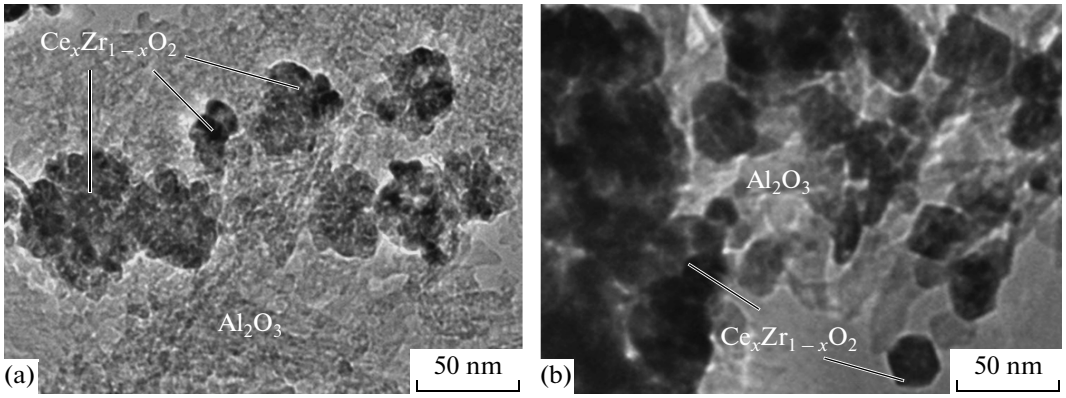

Fig. 4. TEM image of (a) as-prepared A25-CZ and (b) the same material calcined at 1000°C.

Al_2O_3 crystallites that are about 5 nm in size have a uniform crystallographic orientation. The $Ce_xZr_{1-x}O_{2-\delta}$ particles are located on the surface in the form of aggregates with an average size of 50 nm. These aggregates are made up of packed smaller crystallites ~5 nm in size. The $Ce_xZr_{1-x}O_{2-\delta}$ particle size distribution is very wide, ranging from a single crystallite (5 nm) to 500-nm aggregates. Only a small part of the $Ce_xZr_{1-x}O_{2-\delta}$ crystallites is located in the Al_2O_3 bulk; most of them form aggregates similar to those observed in CZ. The composition of the oxide $Ce_xZr_{1-x}O_{2-\delta}$, which was determined for a number of particles, turned out to depend on the particle size. The heat treatment of A10-CZ leads to the sintering of both $Ce_xZr_{1-x}O_{2-\delta}$ and Al_2O_3. As a result, the Al_2O_3 aggregates consist of identically oriented needle crystallites with average dimensions of 50 (length) ×10 (width) nm. As in the case of the as-prepared sample, $Ce_xZr_{1-x}O_{2-\delta}$ is nonuniformly distributed in the Al_2O_3 matrix. The $Ce_xZr_{1-x}O_{2-\delta}$ crystallites in the heat-treated sample have a larger size of 15–20 nm.

As compared to the alumina matrix in A10-CZ, the Al_2O_3 matrix in A25-CZ consists of smaller aggregates (Fig. 4). There are two types of alumina aggregates here: platelike aggregates with a characteristic size of ~10 nm and 5 × (30–70) nm needles. The spatial distribution of $Ce_xZr_{1-x}O_{2-\delta}$ and Al_2O_3 is rather uniform, and the $Ce_xZr_{1-x}O_{2-\delta}$ and Al_2O_3 particles are mixed well. The particle size distribution of $Ce_xZr_{1-x}O_{2-\delta}$ is narrow, lying within the 30–50 nm range, with a mean particle size of ~40 nm. The particles have a defective structure consisting of 8–10 nm crystallites. In rare cases, there are disordered agglomerates of phases up to 500 nm in size. Also observed are separate, unaggregated, ~10-nm $Ce_xZr_{1-x}O_{2-\delta}$ crystallites in contact with Al_2O_3.

The calcination of A25-CZ results in the sintering of alumina. The plate-like Al_2O_3 particles grow to a size of 30–50 nm; the needle particles, to 10–100 nm. The oxide $Ce_xZr_{1-x}O_{2-\delta}$ is represented by two morphological types of particles, namely, 30- to 50-nm single-crystal particles and their 100- to 200-nm aggregates (Fig. 4). Thus, there are single $Ce_xZr_{1-x}O_{2-\delta}$ crystallites distributed in the composite containing about 25 wt % Al_2O_3, but this percentage of Al_2O_3 is apparently insufficient to hamper their agglomeration and coalescence.

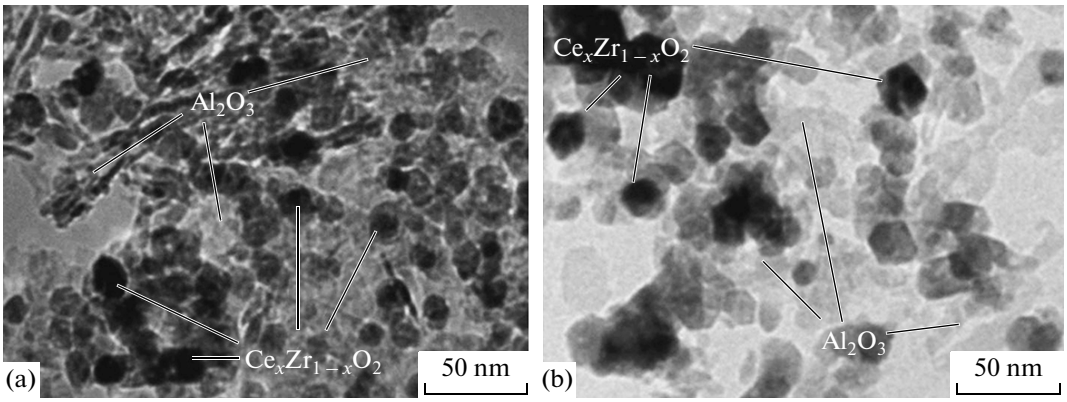

Fig. 5. TEM image of (a) as-prepared A50-CZ and (b) the same material calcined at 1000°C.

In the as-prepared A50-CZ composite, there are almost no alumina aggregates (Fig. 5). Like A25-CZ, this composite contains platelike and needle crystallites. However, the proportion of needle crystallites is considerably smaller in this case. The character of $Ce_xZr_{1-x}O_{2-\delta}$ particle size distribution here is the same as in A25-CZ, but the particle sizes are within the narrower range from 10 to 15 nm (mean particle size of ~12 nm). The $Ce_xZr_{1-x}O_{2-\delta}$ particles in this composite, as distinct from those in A25-CZ, are practically single crystals, although both materials are considered in their as-prepared states. Larger particles (up to 40 nm) can be noticed in some cases. The chemical composition of the $Ce_xZr_{1-x}O_{2-\delta}$ particles is practically uniform, with Ce : Zr ≈ 76 : 24; however, smaller particles contain a larger proportion of Zr.

After the calcination of A50-CZ, the size of its Al_2O_3 crystallites is almost unchanged. As distinct from A25-CZ, this composite contains no large needle particles resulting from coalescence. The $Ce_xZr_{1-x}O_{2-\delta}$ particles in the calcined sample are insignificantly larger than those in the as-prepared sample, and their average size is 15 nm. The number of particle aggregates in the calcined sample is larger, but only slightly (Fig. 5).

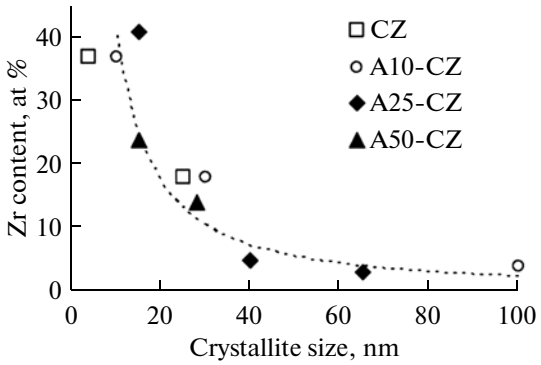

Fig. 6. Weight percent of Zr atoms in the $Ce_xZr_{1-x}O_{2-\delta}$ crystallites versus their size.

A TEM examination of all as-prepared and calcined samples demonstrated that Zr is nonuniformly distributed in the $Ce_xZr_{1-x}O_{2-\delta}$ phase. At least two types of particles are observed, which differ in their size. According to microprobe analysis data, the zirconium content of the crystallites is a decreasing function of their size (Fig. 6). Large crystallites (15–20 nm and above) and smaller ones have a lower and higher Zr content, respectively, relative to the theoretical value 0.25. It is the presence of Zr-enriched particles that is responsible for the appearance of the reflections from the tetragonal ZrO_2 phase in CZ, A10-CZ, and A25-CZ after calcination (Fig. 1). Note that no tetragonal ZrO_2 was detected by X-ray diffraction in the as-prepared samples. However, calcination causes the coalescence of fine particles, and this phase becomes observable.

As a consequence of the nonuniform distribution of Zr, the unit cell parameter of $Ce_xZr_{1-x}O_{2-\delta}$ is larger than its reference value. Its observed value is mainly determined by large particles (tens of nanometers in size) with a low Zr content.

The nonuniform distribution of Zr in the $Ce_xZr_{1-x}O_{2-\delta}$ phase synthesized by direct precipitation is a typical feature arising from the difference between the ZrO^{2+} and Ce^{3+} precipitation pH values ($pH_{ZrO^{2+}}$ 2–3, $pH_{Ce^{3+}}$ 6–8). In addition, as the precipitate is then heat-treated at T = 100°C, the dehydration of cerium and zirconium hydroxides to the respective oxides may proceed at different rates and this may yield an inhomogeneous product. At the same time, the $Ce_xZr_{1-x}O_{2-\delta}$ particles in A50-CZ are single crystals and are practically uniform in chemical composition and size. Apparently, both textural and structural promotion effects take place in the direct precipitation synthesis of the Al_2O_3–$Ce_xZr_{1-x}O_{2-\delta}$ composite containing about 50 wt % Al_2O_3.

The nonuniformity of Zr distribution in the $Ce_xZr_{1-x}O_{2-\delta}$ particles, established for the CZ, A10-CZ, and A25-CZ composites, affects crystallite size

measurements by X-ray diffraction. Because of the closeness of the reflections from different $Ce_xZr_{1-x}O_{2-\delta}$ phases similar in chemical composition, these reflections overlap and some of them broaden, distorting the crystallite size data calculated via the Scherrer formula. Here, TEM data are more appropriate for estimation of the crystallite size. For the A50-CZ composite, which is made up of monodisperse crystallites with similar chemical compositions, the TEM and X-ray diffraction methods give similar crystallite size values.

The presence of the Zr-rich phase in A10-CZ and A25-CZ must exert a favorable, stabilizing effect on alumina, since zirconium introduced in Al_2O_3 inhibits phase transition and the formation of α-Al_2O_3 with a small specific surface area [10, 11]. Nevertheless, TEM data do not confirm the stabilizing effect of $Ce_xZr_{1-x}O_{2-\delta}$ on Al_2O_3 in these materials: Al_2O_3 is present in the form of aggregates and calcination yields large needle particles. This can lead to further α-Al_2O_3 formation. The oriented growth of the alumina needles is restricted in the case of the homogeneous mixing of the $Ce_xZr_{1-x}O_{2-\delta}$ crystallites on Al_2O_3, which is observed in A50-CZ.

Temperature-Programmed Reduction with Hydrogen

The reduction sequence for the cerium-containing materials was studied by TPR with hydrogen. The TPR spectrum of CZ has a complicated shape (Fig. 7). The reduction of the material occurs in two stages, as is indicated by the existence of two peaks in the TPR curve at ≈550°C and ≈800°C. In the same spectrum of CeO_2, the lower temperature peak is due to the reduction of Ce^{4+} cations on the surface and the higher temperature peak is due to Ce^{4+} reduction in the bulk [20]. As the proportion of Zr in the oxide is increased, the temperature of the reduction of the sample with hydrogen decreases. The lower temperature peak is asymmetric, and its left shoulder, occurring at 400–500°C is assignable to the reduction of the fine-particle $Ce_xZr_{1-x}O_{2-\delta}$ phase enriched with zirconium.

With an increasing amount of Al_2O_3 in the composite, the H_2 uptake peak corresponding to bulk reduction weakens and shifts to lower temperatures in the following order: A10-CZ, 750°C; A25-CZ, 720°C; A50-CZ, 600–610°C.

The A10-CZ composite is characterized by two separate low-temperature peaks at 475 and 554°C, which are due to the reduction of $Ce_xZr_{1-x}O_{2-\delta}$ oxides differing in their chemical composition and particles size, as was observed by the X-ray diffraction and TEM methods.

The reduction of A25-CZ includes at least three stages, as is indicated by the corresponding peak having a left and a right shoulder. As compared to the peak of A10-CZ, the unresolved peak at ≈475°C is weaker. This may be due to the smaller proportion of the fine-particle, zirconium-enriched fraction. This hypothesis is corroborated by TEM (Fig. 4) and X-ray diffraction (Fig. 1), which visually indicate a smaller proportion of finely dispersed particles and a lower intensity of the ZrO_2 (111) reflection after calcination.

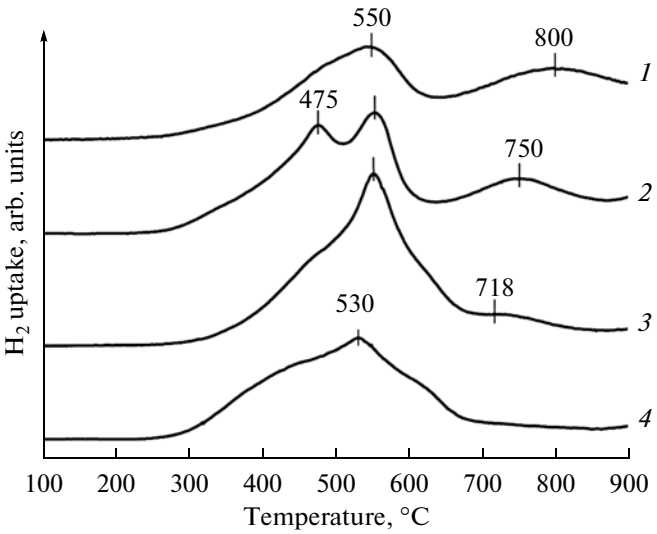

Fig. 7. TPR spectra of the (*1*) CZ, (*2*) A10-CZ, (*3*) A25-CZ, and (*4*) A50-CZ composites.

The reduction of A50-CZ also takes place in three stages, with a peak occurring at 530°C. The reduction peaks are unresolved, as in the case of A25-CZ, but they are lower and are shifted to lower temperatures by approximately 20–40°C. The fact that the reduction temperature of A50-CZ is lower than that of the other materials is explained by the smaller proportion of large particles with a low Zr content and by the more uniform distribution of Zr in the CeO_2 crystal lattice in this sample, as follows from our TEM (Fig. 5) and X-ray diffraction (Fig. 1) data.

With an increasing proportion of Al_2O_3 in the composite, the amount of hydrogen consumed in reduction practically does not change (Table 2), but the hydrogen uptake in the low-temperature region increases. The boundary between the low- and high-temperature regions was determined from the TPR spectrum of CZ as the minimum between the first and second peaks (~650°C). Taking into account that the aluminum and zirconium cations do not undergo reduction, we calculated the hydrogen uptake per unit weight of CeO_2. It can be seen that that the reducibility of cerium increases significantly with an increasing Al_2O_3 content; up to 650°C, this parameter of A50-CZ is almost 3 times larger than that of CZ. This correlates well with the observation that the size of the $Ce_xZr_{1-x}O_{2-\delta}$ aggregates decreases as the proportion of Al_2O_3 in the composite is increased, thus increasing the number of surface atoms of cerium.

Table 2. TPR data for the composites

Parameter	Composite			
	CZ	A10-CZ	A25-CZ	A50-CZ
Hydrogen uptake up to 900°C:				
mmol H_2/g sample	1.08	1.09	1.12	0.90
mmol H_2/g CeO_2	1.35	1.51	1.82	2.08
Hydrogen uptake up to 650°C:				
mmol H_2/g sample	0.59	0.72	0.87	0.90
mmol H_2/g CeO_2	0.74	1.00	1.41	2.08

Oxygen Storage Capacity

The dynamic OSC data obtained for the monolith samples in the flow reactor are presented in Fig. 8. For all composites, the OSC data are plotted versus temperature in the 200–500°C range as a saturation curve tensing to a limiting value. The curves for CZ and A25-CZ begin at approximately equal temperatures about 240°C and almost coincide up to 400°C. At higher temperatures, the OSC of CZ exceeds that of A25-CZ (Fig. 8). The closeness of the OSC values of these materials is in agreement with the identity of the morphologies and chemical compositions of the $Ce_xZr_{1-x}O_{2-\delta}$ particles in the calcined samples (TEM data).

The OSC of A10-CZ is slightly lower than that of CZ and A25-CZ throughout the temperature range examined (Fig. 8). It follows from the X-ray diffraction, TEM, and TPR data that A10-CZ has the most nonuniform distribution of $Ce_xZr_{1-x}O_{2-\delta}$ particles over chemical composition and size. The systems with an inhomogeneous Zr distribution, which consist of a variety of $Ce_xZr_{1-x}O_{2-\delta}$ phases differing in composition, are known to have a lower OSC than the cubic solid solution with a uniform Ce and Zr distribution [21, 22].

The OSC of A50-CZ shows itself at a lower temperature than the OSC of the other materials and has a larger value throughout the temperature range examined. The OSC of this composite reaches its limit above 300°C and then remains practically invariable up to 500°C. The absence of large $Ce_xZr_{1-x}O_{2-\delta}$ aggregates and the persistence of the fine crystallites in A50-CZ upon calcination suggests that this material has a larger proportion of surface cerium. Firstly, this can actually be seen from the TPR spectrum as the

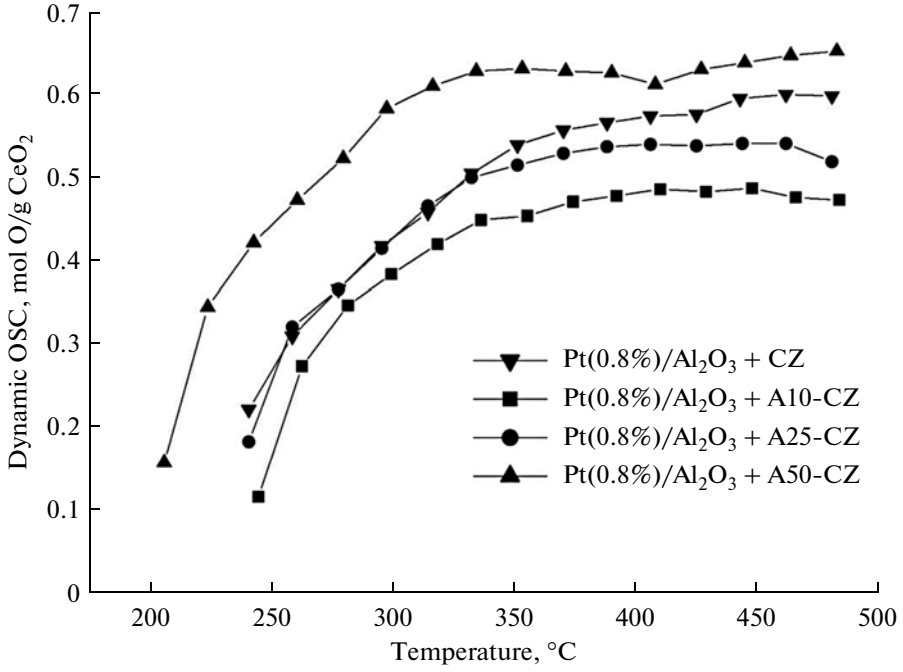

Fig. 8. Dynamic OSC as a function of temperature for the Pt(0.8%)/Al_2O_3 + Al_2O_3–$Ce_xZr_{1-x}O_{2-\delta}$ catalysts. The Al_2O_3–$Ce_xZr_{1-x}O_{2-\delta}$ composites were aged at 1050°C.

Table 3. Temperatures of 50% conversion

Component	T_{50}, °C			
	Pt/Al_2O_3 + CZ	Pt/Al_2O_3 + A10-CZ	Pt/Al_2O_3 + A25-CZ	Pt/Al_2O_3 + A50-CZ
CO	267	244	227	200
CH_x	287	278	272	249
NO_x	281	271	262	247

absence of the high-temperature peak due to the reduction of bulk cerium at 800°C (Fig. 7); secondly, this is favorable for the manifestation of low-temperature dynamic OSC (Fig. 8). According to TEM data, upon calcination the $Ce_xZr_{1-x}O_{2-\delta}$ particles in this material retain their homogeneous composition close to the theoretical composition (Ce : Zr = 75 : 25). Because of this, the dynamic OSC of A50-CZ is highest in the composite series.

Catalytic Activity

The catalytic activity data for the monoliths containing the oxides examined are presented in Table 3. The 50% CO, CH_x, and NO_x conversion temperature for the $Pt(0.8\%)/Al_2O_3$+Al_2O_3–$Ce_xZr_{1-x}O_{2-\delta}$ catalysts decreases with an increasing proportion of Al_2O_3 in the composite. Thus, an increase in catalytic activity correlates with an increase of the degree of dispersion of the cerium-containing particles. The lowest 50% conversion temperatures were observed for the catalyst that contains the A50-CZ composite and has the highest OSC.

CONCLUSIONS

As a step in development of a thermally stable Al_2O_3–$Ce_{0.75}Zr_{0.25}O_2$ composite system for three-way catalysts, we prepared a series of materials containing 0, 10, 25, and 50% Al_2O_3 and catalysts based on these materials. The materials were characterized by a complex of physicochemical methods, and activity characteristics of the catalysts were measured. It was established that the cubic solid solution $Ce_xZr_{1-x}O_{2-\delta}$ is present is all of the synthesized materials. However, the uniform distribution of Zr is not ensured at alumina contents of 0, 10, and 25%. The zirconium content of the $Ce_xZr_{1-x}O_{2-\delta}$ crystallites varies antibatically with their size. As the percentage of alumina in Al_2O_3–$Ce_{0.75}Zr_{0.25}O_2$ is increased, large $Ce_xZr_{1-x}O_{2-\delta}$ aggregates disappear and the proportion of small $Ce_xZr_{1-x}O_{2-\delta}$ particles increases. Practically single-crystal, 12- to 17-nm $Ce_{0.75}Zr_{0.25}O_2$ particles similar in chemical composition form in the composite containing 50 wt % Al_2O_3, and these particles remain almost unchanged upon calcination at 1000°C. The uniform mixing of Al_2O_3 and $Ce_{0.75}Zr_{0.25}O_2$ particles on the nanometer scale enhances the sintering resistance of the composite. Alumina serves as a structural promoter and diffusion barrier for the $Ce_{0.75}Zr_{0.25}O_2$ particles. In addition, single-crystal $Ce_{0.75}Zr_{0.25}O_2$ particles block the oriented growth of Al_2O_3 particles during calcination.

The increase in the degree of dispersion of $Ce_xZr_{1-x}O_{2-\delta}$ in the composite series causes an increase in the number of surface cerium atoms. This enhances the low-temperature reducibility of the composite. The higher OSC of the calcined composite containing 50 wt % Al_2O_3 is evidence that this material has a larger proportion of cerium atoms capable of participating in the redox process.

In the composite series examined, the promoting effect of the introduction of alumina in Al_2O_3–$Ce_xZr_{1-x}O_{2-\delta}$ coprecipitation is most pronounced at an Al_2O_3 content of 50 wt %. The results of the promoting effect are the increased thermal stability, high OSC, and high activity of the catalysts supported on this composite. This makes the composite promising for catalysts operating at high temperatures, including in three-way catalytic converters for internal-combustion engines.

REFERENCES

1. Gandhi, H.S., Graham, G.W., and McCabe, R.W., *J. Catal.,* 2003, vol. 216, p. 433.
2. Favre, C. and Zidat, S., *SAE Tech. Paper Ser.* 2004-01-0138, 2004.
3. Perrichon, V., Laachir, A., Abouarnadasse, S., Touret, O., and Blanchard, G., *Appl. Catal., A,* 1995, vol. 129, p. 69.
4. Ivanov, V.K., Polezhaeva, O.S., Baranchikov, A.E., and Shcherbakov, A.B., *Inorg. Mater.,* 2010, vol. 46, no. 1, p. 43.
5. Trovarelli, A., *Catal. Rev. Sci. Eng.,* 1996, vol. 38, p. 439.
6. Madier, Y., Descorme, C., Le Govic, A.M., and Duprez, D., *J. Phys. Chem. B,* 1999, vol. 103, p. 10999.
7. Fornasiero, P., Di Monte, R., Ranga Rao, G., Kaspar, J., Meriani, S., Trovarelli, A., and Graziani, M., *J. Catal.,* 1995, vol. 151, p. 168.
8. Cuif, J.P., Blanchard, G., Touret, O., Seigneurin, A., Marczi, M., and Quemere, E., *SAE Tech. Paper Ser.* 970463, 1997.
9. Bozo, C., Gaillard, F., and Guilhaume, N., *Appl. Catal., A,* 2001, vol. 220, p. 69.

10. Burtin, P., Brunelle, J.P., Pijolat, M., and Soustelle, M., *Appl. Catal.,* 1987. vol. 34. p. 225.
11. Ismagilov, Z.R., Shkrabina, R.A., Koryabkina, N.A., Arendarskii, D.A., and Shikina, N.V., *Stud. Surf. Sci. Catal.,* 1998, vol. 116, p. 507.
12. Chuech, J.S. and Cant, N.W., *Appl. Catal., A,* 1993, vol. 101, p. 105.
13. Monte, R.D., Fornasiero, P., Kaspar, J., and Graziani, M., *Stud. Surf. Sci. Catal.,* 2001, vol. 140, p. 229.
14. Wei, Z., Li, H., Zhang, X., Yan, S., Zhen, L., Chen, Y., and Gong, M., *J. Alloys Compd.,* 2008, vol. 455, p.322.
15. Yao, M.H., Baird, R.J., Kunz, F.W., and Hoost, T.E., *J. Catal.,* 1997, vol. 166, p. 67.
16. Morikawa, A., Suzuki, T., Kanazawa, T., Kikuta, K., Suda, A., and Shinjo, H., *Appl. Catal., B,* 2008, vol. 78, p. 210.
17. Chuang, C., Hsiang, H., Hwang, J.S., and Wang, T.S., *J. Alloys Compd.,* 2009, vol. 470, p. 387.
18. Porsin, A.V., Alikin, E.A., Danchenko, N.M., Rychkov, V.N., Smirnov, M.Yu., and Bukhtiyarov, V.I., *Katal. Prom–sti.,* 2007, no. 6, p. 39.
19. Speight, J.G., *Lange's Handbook of Chemistry,* New York: McGraw-Hill, 1999, 16th ed.
20. Yao, H.C. and Yu, Y., *J. Catal.,* 1984, vol. 86, p. 254.
21. Nagai, Y., Nonaka, T., Suda, A., and Sugiura, M., *R&D Rev. Toyota CRDL,* 2002, vol. 37, no. 4, p. 20.
22. Hori, C.E., Permana, H., Ng, K.Y.S., Brenner, A, More, K., Rahmoeller, K.M., and Belton, D.N., *Appl. Catal., B,* 1998, vol. 16, p. 105.

Translated by D. Zvukov